Investigation of a New Application for Cellulose Nanocrystals – A Study of the Enhanced Oil Recovery Potential by use of a Green Additive

Authors: Silje N. Molnes[a,b], Aleksandr Mamonov[a], Kristofer G. Paso[b], Skule Strand[a], Kristin Syverud[b,c,*]

[a] *Department of Petroleum Technology, University of Stavanger (UoS), 4036 Stavanger, Norway*

[b] *Department of Chemical Engineering, Norwegian University of Science and Technology (NTNU), 7491 Trondheim, Norway*

[c] *RISE PFI, Høgskoleringen 6B, 7491 Trondheim, Norway*

*Corresponding author**.**
E-mail address: kristin.syverud@rise-pfi.no (K. Syverud)
Phone: +47 959 03 740

Key words:
Nanocellulose
Stability
Oil recovery
CNC
Temperature
Heat aging

Abstract

Cellulose nanocrystals (CNC) has been investigated for a potential new application, enhanced oil recovery (EOR), by performing core flooding experiments with CNC dispersed in low salinity brine (CNC-LS) in outcrop sandstone cores. Experiments on 100 % water saturated cores confirmed that most of the viscosity generating CNC particles were able to travel through the cores at temperatures ranging from 60, to 120 °C. Oil recovery experiments on crude oil saturated sandstone cores showed that when CNC-LS was used in tertiary mode, the ultimate oil recovery could be increased, both at 90 and 60 °C. During tertiary CNC-LS injection, the CNC particles increased fluctuations in differential pressure, an effect that can be linked to log jamming in pore throats leading to remobilisation of oil in the pore space. The results from this work indicate that CNC dispersed in low saline brine might have a certain potential for use in enhanced oil recovery.

1. Introduction

The world is experiencing an ever-increasing energy demand, and although there is a lot of focus on the “green shift”, with energy originating from renewable sources, one cannot avoid the fact that petroleum-derived products will continue to be an important part of everyday life.

Many of the oilfields around the world are approaching, or is in the phase where the rate of production is declining (Hendraningrat et al., 2013). The average oil recovery from mature oilfields is between 20 and 40 %, meaning that as much as 60 – 80 % of the original oil in place (OOIP) remains in the reservoirs after conventional recovery methods are spent. Even with the current situation, with relatively low oil prices, an increase of a few percent of OOIP might be economically viable compared to exploration and drilling of new wells. It is becoming more and more difficult to discover new oilfields suitable for production, and many of these unexplored fields are located in remote and/or environmentally vulnerable areas (Muggeridge et al., 2014).

Oil is recovered by creating pressure gradients, which causes the oil to flow towards a production well. In primary or first-line recovery, this process is mostly driven by natural flow, sometimes assisted by artificial lift. Secondary oil recovery is usually assisted by gas-injection or water-flooding, through injection wells for offshore reservoirs, and most often with seawater (Muggeridge et al., 2014; Thomas, 2008; Wei et al., 2016). The injection fluid has low viscosity compared to the oil phase which reduces the total sweep efficiency (Liu et al., 2012). The ultimate oil recovery is determined by two different efficiencies; the microscopic displacement efficiency, which is a measure of oil recovery at pore level. Due to wetting and capillary trapping of oil in pore spaces, this efficiency rarely exceeds 70 % OOIP (Hu et al., 2016). The second determinant is the macroscopic sweep efficiency, which refers to the amount of oil the

flooding fluid can contact. Technologies that improve these two parameters are usually referred to as tertiary, or enhanced oil recovery (EOR) (Taber et al., 1997).

The term EOR comprises many different techniques, but in this paper the focus will be on chemical methods, through alteration of the ion composition of the injection brine, and nanoparticle flooding. The addition of polymers to the flooding fluid increases the viscosity of the aqueous phase, thus lowering the mobility ratio between the water and oil phases. This could be a favourable situation, by improving both the vertical- and area sweep efficiency (Raney et al., 2012). Polymer flooding has been thoroughly researched and implemented in fields for the last 40 years (Kamal et al., 2015). Two types of polymers are more extensively utilised than others. These are the synthetic hydrolysed polyacrylamides (HPAMs) and the polysaccharide biopolymer xanthan gum. HPAMs is most often used due to low cost and improved viscoelastic properties compared to xanthan gum (Sheng et al., 2015). Both polymers have some drawbacks though; HPAMs are generally not very stable in high salinity dispersions and at elevated reservoir temperatures, in addition to being susceptible to shear degradation (Raney et al., 2012). Xanthan gum tolerates high salinity and shear forces, but has relatively low temperature stability (Seright & Henrici, 1990) and problems with formation plugging, viscosity loss and bacterial degradation has been experienced (Wellington, 1983). The problem with biodegradation is that biocides need to be added to the polymer injection brine, which may cause an otherwise environmentally friendly polymer to become harmful to the environment. HPAM also has some problems due to poor biodegradation properties, making it necessary with post-flooding water treatment, which might be costly, time consuming and poses an environmental threat if it fails (Guo, 2013). There is also some suspicion regarding its breakdown into toxic acrylamide after slow natural degradation, which can cause harm to local ecosystems (Aguiar & Mansur, 2016; Bao et al., 2010).

Cellulose nanocrystals (CNC) is here introduced as a potential green alternative to water assisted polymer flooding. CNC is rod-like particles derived from cellulose of various sources, most often wood, through controlled acid hydrolysis (Klemm et al., 2011). Coming from an abundant and completely renewable source, CNC is both non-toxic and biodegradable, making it a green flooding chemical according to the OSPAR Commissions PLONOR list (OSPAR, 2016). CNC particles from wood are usually 3 – 5 nm wide and have lengths ranging from 100 – 200 nm (Habibi et al., 2010). They do not alter the viscosity of the injection brine significantly, and are added to improve the microscopic and macroscopic sweep efficiencies through flow diversion. As is the case with the particles used in the experiments in this article, CNC is often produced using 64 wt. % sulphuric acid at a temperature of 45 °C, with reaction times depending on the temperature used (Reiner & Rudie, 2013). The acid reacts with the hydroxyl groups on the surface of the cellulose, which removes the amorphous part of the cellulose and yields crystalline CNC particles with charged sulphate half esters on

the surface. This leaves the particles anionic, promoting their dispersion behaviour in water (Revol et al., 1992). The use of cellulose nanocrystals for petroleum industry applications is not a complete novelty, it has been used as cement strengthener, by adding it to well fluids, and it has been used to increase the viscosity of water-based well fluids for fracturing and gravel packing (Rincon-Torres & Hall, 2015). Proposals have also been made to utilise CNC in well treatment fluids as a substitute for conventional polymers (Lafitte et al., 2014). No reports have been found of the use of CNC in enhanced oil recovery, but cellulose derivatives like variations of hydrophobically modified hydroxyethyl cellulose (HM-HEC) have been investigated, although these, like HPAMs have shown to be relatively salt sensitive (Kjøniksen et al., 2008; Wever et al., 2011). Cellulose nanocrystals are believed to be less vulnerable to shear and biological degradation due to their crystalline morphology (Aadland et al., 2016), and has a thermal stability within the limits for oilfield applications (Heggset et al., 2017; Molnes et al., 2017).

Presented in this paper is a lab scale study of the EOR potential in sandstone of negatively charged cellulose nanocrystals used in combination with low salinity (LS) brine. The stability of CNC in dispersions with low salinity (1000 ppm NaCl) brine has been investigated and proved earlier (Molnes et al., 2016). Flooding procedures are performed using CNC in combination with low saline brines which changes the wettability and redistributes the residual oil within the pore spaces of the sandstone cores. CNC has also been subjected to core flooding procedures at lab scale to investigate the injectivity and eventual retention of CNC inside sandstone cores. These investigations have shown that the CNC is injectable in sandstone and are able to travel through the core, but some filtering and retention of larger particles was observed. These effects were enhanced when the CNC concentration or the brine injection rate was increased (Aadland et al., 2016; Molnes et al., 2016).

A proposed mechanism for CNC in a porous media is log-jamming, where the particles block pore throats (larger than the particle size) and thus cause microscopic diversion in the pore matrix. The most important factors regarding log-jamming are pore size distribution, particle concentration and effective hydrodynamic size, as well as the injection flow rate (Bolandtaba et al., 2009; T. Skauge et al., 2010).

The pore-jamming effect can partly be explained by the mass difference between the particles and the dispersion medium. Pore throats are smaller than the pores, and combined with the constant differential pressure, the flow velocity will increase at the pore throats compared to inside the pores. Water molecules will accelerate faster than the particles at the entrance of a pore throat, due to a significant difference in mass between a water molecule and a particle. The particles will then start to accumulate at the pore throat and slowly reduce the diameter of the pore throat and eventually block it.

The initial wetting properties of an oil reservoir is related to the chemical equilibrium between rock surface, oil phase and brine phase, which is established over millions of years. The extremes are completely oil or completely water wet, and a typical sandstone reservoir is usually mixed wet. Improvement of the oil recovery from a reservoir in equilibrium is possible through alteration of the ionic composition of the injected brine, which will destabilise the system and increase the oil flow through the porous formation (Strand et al., 2016). The effect of low saline brine flooding on enhanced oil recovery has been known for many years, and it has also been confirmed experimentally and in the field (Lager et al., 2007; Seccombe et al., 2010; Tang & Morrow, 1999a, 1999b). It is generally accepted that the effect of the LS brine flooding in sandstone reservoirs is caused by a wettability alteration of the sandstone, but there is still some debate regarding how this wettability modification takes place (Strand et al., 2016). Over the years, a variety of mechanisms has been proposed: 1) Migration of fines from clay (Tang & Morrow, 1999a), 2) Increase in pH due to impact from alkaline flooding (McGuire et al., 2005), 3) Multi-component ion exchange (MIE) at the clay surface (Lager et al., 2007), 4) Migration of fines causing microscopically diverted flow (A. Skauge, 2008), and 5) Ionic double layer expansion at the rock surface (Ligthelm et al., 2009). Austad et al. (2010) described a new mechanism, based on, and in agreement with existing experimental data. At reservoir conditions, the pH value of the formation water (FW) is slightly acidic, due to dissolved acidic gases like H_2S and CO_2. Negatively charged mineral surfaces like clay work as a cation exchange material, and will at this pH adsorb acidic and protonated basic components from the crude oil, as well as cations like Ca^{2+} from the formation water. When low salinity brine is injected into this system, a desorption of Ca^{2+} from the clay surface is promoted, which will lead to a local pH increase in the interface between the clay and LS brine because Ca^{2+} is substituted by H^+ from the injected fluid. A fast reaction between OH^- and the adsorbed acidic and protonated basic material leads to a desorption of organic material from the clay, causing an improved water wetness, which generate positive capillary forces and enhance the oil recovery (Austad et al., 2010).

It is experimentally verified in oil recovery experiments from restored cores that FW injection, which will not chemically affect the initial core wettability established, gives a low oil recovery, typically ~40 % OOIP (Piñerez Torrijos et al., 2016; Torrijos et al., 2017).The FW injection is successively followed by tertiary LS injection which significantly improves the oil recovery with 8-9 % OOIP, which could only be explained by a wettability alteration towards more water wet conditions and is also confirmed in Spontaneous Imbibition (SI) experiments. Using the same Crude oil-Brine-Rock system (CoBR), a secondary LS injection improved the oil recovery to 66 % OOIP compared to only 40 % OOIP with FW (Piñerez Torrijos et al., 2016). The secondary flooding with LS brine will cause a wettability change in the pore matrix of the sandstone core, and redistribute the residual oil to the middle of the pores making it

more accessible for EOR techniques. Tertiary injection of CNC may cause log-jamming of pore throats and divert the water flow into the lesser available, oil containing pores to further increase the oil recovery.

This paper describes core flooding tests that have been performed on outcrop sandstone cores, saturated with LS brine, at temperatures from 60 to 120 °C, while the oil recovery tests were performed on outcrop sandstone cores at 60 and 90 °C. Testing at such elevated temperatures is relevant due to the temperatures encountered in oil reservoirs. Reservoir temperatures increases with burial depth, usually with 3 °C per 100 m depth, with temperatures reaching above 150 °C (Beal, 1946; Jahn et al., 2008). The cores in the oil recovery tests were restored with initial water saturation (S_{wi}) of 0.2, saturated and aged in crude oil. The cores have been successively flooded, first with LS brine, followed by LS brine with CNC. Both oil recovery and differential pressure over the core have been monitored during the tests.

2. Materials and Methods

2.1 Materials

Cellulose nanocrystals

Cellulose nanocrystals (CNC) were acquired from the Process Development Centre at The University of Maine (USA). The particles were produced by the Forest Products Laboratory (FPL), USDA (US: Department of Agriculture) by acid hydrolysis of softwood pulp using 64 % (by mass) sulphuric acid. CNC from the same provider was analysed by Sacui et al. (2014) by transmission electron microscopy (TEM) and atomic force microscopy (AFM). The charge density of the sulphate ester groups was evaluated by Heggset et al. (2016). All values are shown in Table 2.1.

Table 2.1: CNC characteristics, adapted from (Heggset et al., 2017) and (Sacui et al., 2014).

Sample	Charge density (mmol/g)	Crystallite diameter (nm)[c]	Crystallite length (nm)[c]	Functional groups
CNC	approx. 0.3[a,b]	5.9 ± 1.8	130 ± 67	-OH, -SO_3H

[a]Amount of sulphate ester groups
[b]Measured with inductively coupled plasma-atomic absorption (ICP-AA) (Heggset et al., 2017).
[c]Determined with atomic force microscopy (AFM) (Sacui et al., 2014).

The dispersion stability of CNC particles at elevated temperatures has been investigated at an earlier point (Heggset et al., 2017; Molnes et al., 2017), and the particles are regarded as relatively stable in low saline dispersions at the temperatures and time frames used in the

experiments performed for this article. However, the colloidal stability of CNC is to some degree affected by electrolytes. Zhong et al. (2012) have reported that the zeta potential of CNC dispersions was reduced to below -30 mV and that the particles started to agglomerate at Na^+ concentrations from 10 mM (Zhong et al., 2012). High temperatures will also cause desulfation of CNC with reduced surface charge and less colloidal stability as a result (Dorris & Gray, 2012).

Brines

Brines were prepared using de-ionized (DI) water and reagent grade chemicals as given in Table 2.2. After adding the salts, the brine solutions were stirred for approximately one hour, before being filtrated over 0.22 µm Millipore filter paper. Formation water (FW) brine was diluted five times with DI water and will from now be denoted d_5FW. The finished brines were stored at room temperature. CNC dispersions were prepared by adding exact amounts of CNC to LS brine to achieve a concentration of 0.5 wt. %; before the dispersions were vigorously shaken until the particles were well dispersed in the brine. The salinity contribution by Na^+ present in the CNC particles was not considered, as Na^+ only exists in CNC in minuscule amounts.

Table 2.2: Brine compositions. TDS = total dissolved solids.

Ions	FW (mM)	d_5FW (mM)	LS (mM)
Na^+	1540	308	17
Cl^-	1720	356	17
Ca^{2+}	90	24	-
TDS (mg/L)	**100 000**	**20 000**	**1000**

Core material

Two cylindrical outcrop sandstone cores were utilised in the experiments, and are denoted SM8 and SM10, respectively. The mineralogical properties have earlier been investigated through X-ray diffraction analysis (XRD), and are given in Table 2.3.

Table 2.3: Mineralogical properties of the outcrop sandstone cores used in the experiments, given in wt. %.

Albite	Quartz	Calcite	Apatite	Pyrite	Anatase	Chlorite	Illite	Clays & micas
32.0	57.0	0.3	0.2	0.1	0.5	1.9	8.6	10.5

The physical properties of the cores are provided in Table 2.4.

Table 2.4: Physical core properties

Core name	Length, cm	Diameter, cm	Dry weight, g	Sat. weight, g	Porosity, %	PV, mL
SM8	7.05	3.79	164.37	180.73	20.33	16.17
SM10	7.04	3.80	165.79	182.33	20.47	16.34

The pore distribution of the core material has been investigated by mercury injection (MICP), confirming heterogeneous pore distribution, Fig. 2.1.

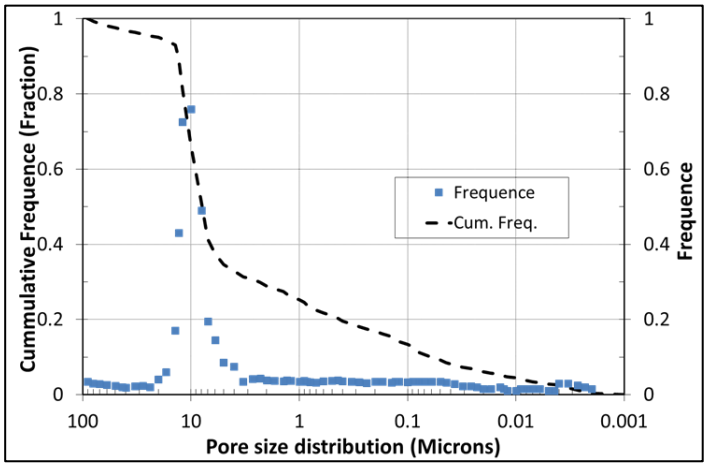

Figure 2.1: Pore size distribution tested by Mercury injection (MICP) into a core from the same block as the tested core material. The core material has a heterogeneous pore size distribution, with pores ranging from ~0.01 to 100 µm. The majority of the pores are in the range of 10 µm.

The same outcrop core material has been used in previous EOR and LS brine studies with very good experimental reproducibility between individual cores (Piñerez Torrijos et al., 2016; Torrijos et al., 2017).

Crude oil

Stabilised crude oil was centrifuged at high rotation speed for 1 hour and filtrated through 8 µm Millipore filter and at last with a 5 µm filter to remove particles and precipitates. The acid number (AN) characterises crude oil through the total concentration of strong and weak acidic organic compounds, and is given as the amount of potassium hydroxide (KOH) needed to neutralise the acids in one gram of oil. The base number (BN) is a measure of the alkalinity of crude oil, given in mg KOH/g crude oil. Both values were acquired by potentiometric titration based on modified versions of ASTM (American Society for Testing Materials) D2896 for BN and ASTM D664 for AN ((ASTM), 1988, 1989; Fan & Buckley, 2006). The crude oil properties are given in Table 2.5.

Table 2.5: Crude oil properties

Acid number (AN) mg KOH/g	Base number (BN) mg KOH/g	Density g/cm^3 at 20 °C	Viscosity, cP at 20 °C
0.1	1.8	0.8459	17.6

2.2 Methods

Core cleaning

A mild core cleaning procedure was used. The core was first flooded with kerosene to displace any residual crude oil from the core. Then followed heptane to displace the kerosene, and at last the core was flooded with 1000 ppm NaCl brine for a few pore volumes (PV), to displace brine and easily dissolvable salts. After this, the core was dried at 90 °C to a constant weight.

Core restoration

Initial water saturation (S_{wi}) of 20 % was established in the mildly cleaned and dried core. The core was saturated under vacuum with 5 times diluted FW (d_5FW). 20 % S_{wi} with FW was established using the desiccator technique (Springer et al., 2003).

Oil saturation and core aging. The core with S_{wi} = 20 % was mounted in a core holder. Gas was removed from the pores by vacuum evaporation, and the core was saturated with crude oil. The core was then flooded with 2. PV of the filtrated crude oil in both directions at 50 °C. The core was then placed in an aging cell and aged for 14 days at the test temperature (60 or 90 °C) before oil recovery experiments were performed. .

Oil recovery experiment

The oil recovery experiment was performed in a computer controlled setup with a Gilson HPLC 307 pump, stainless steel piston cells with either LS brine or CNC-LS brine dispersion. The Hassler core holder was placed in a heating cabinet with gauges for monitoring the inlet and differential pressure (ΔP), as well as the temperature. All experiments were performed with a confining pressure of 20 Bar and a back pressure of 10 Bar. A schematic overview of the core flooding setup can be seen in Figure 2.2.

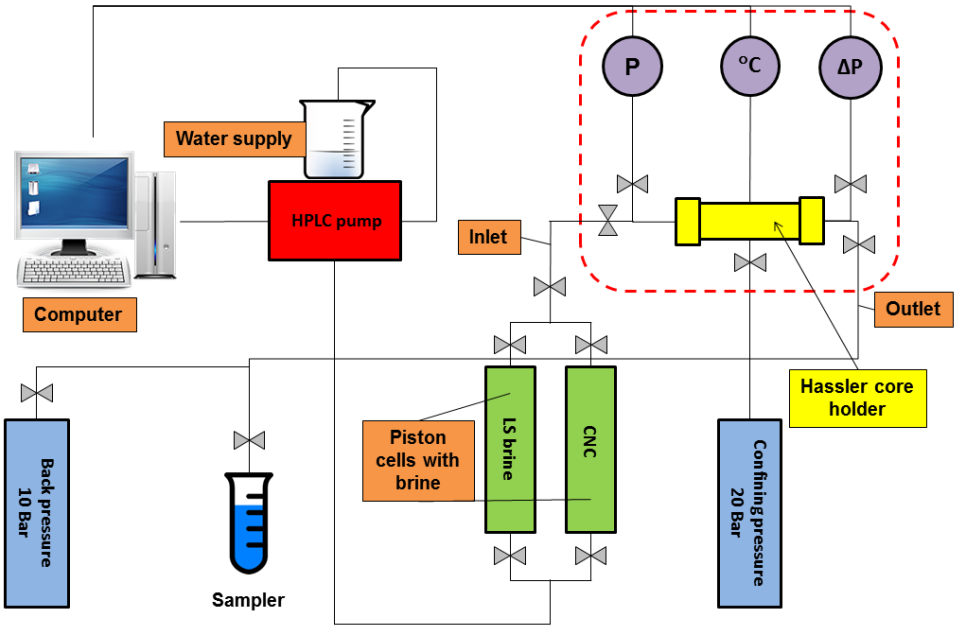

Figure 2.2: Core flooding setup. Line valves are shown in grey, and were used to regulate line flow. The stapled line indicates the heating cabinet.

The restored core was placed in the core holder. The core was equilibrated at test conditions overnight with bypass flow (no fluid flooded through the core) to ensure stable temperature and pressure as well as air tight flood lines prior to testing. The core was successively flooded with LS brine and CNC-LS dispersion at a rate of 4 PV/day. Produced oil and water was monitored and collected using a glass burette and a Gilson GX-271 Liquid Handler (Gilson Inc., Middleton, WI, USA) by night.

CNC injectivity and core permeability

The core permeability was measured on a 100% water saturated core by flooding LS brine at increased flood rate to acquire stable and accurate differential pressure (ΔP) measurements. This was performed before injecting CNC-LS dispersion and then between every temperature step.

Permeability is calculated using the Darcy equation (Eq. 2.1) and given in milliDarcy (mD) (Zolotukhin & Ursin, 2000):

$$k = \frac{\mu \Delta x}{A} \frac{u}{\Delta P} \tag{2.1}$$

Where

μ Viscosity of the injected fluid (for water at 60 °C = 0.47 mPa·s)

Δx Length of sandstone core sample (cm)

A Cross sectional area of sandstone core sample (cm^2)

u Flow rate of the injected fluid (mL/min)

ΔP Differential pressure over the sandstone core sample (mBar)

The oil recovery experiments were performed in the same core flooding setup, using crude oil saturated core SM10 with S_{wi} = 20 %, at 60 and 90 °C. The core was cleaned and restored prior to each EOR test.

Effluent characterisation

The viscosity of brine and the effluent CNC-LS samples was assessed using an Anton Paar MCR 301 rotational rheometer. The instrument was configured with a 50 mm 1° cone and plate geometry with a measuring gap of 0.096 mm. Measurements were performed at 20 °C, with shear rates from 10 – 1000 1/s, and were monitored and logged using the Rheoplus software v3.40.

pH values of LS and CNC-LS effluent samples were measured with a Mettler Toledo SevenEasy™ pH meter.

3. Results and Discussion

3.1 CNC Injectivity study

The injectivity of CNC into sandstone cores was investigated. LS brine with 0.5 wt. % CNC was injected at constant temperature into a 100 % LS saturated outcrop sandstone core SM8 at a flooding rate of 4 PV/day. The inlet pressure and differential pressure over the core was monitored throughout the whole experiment and effluent samples were collected. In between each experiment, the core was cleaned by injection of LS brine in the opposite direction, until stable pressure drop. Experiments were performed at constant temperature, 60, 90 and 120 °C.

The core flooding at 60 °C had an initial ΔP of 6 mBar (100 % LS brine saturation), and the pressure drop gradually increased to 15 mBar after 1 PV injected and continued to increase. After 7 PV, the ΔP had increased to 60 mBar. Viscosity measurement on effluent samples showed only a very small reduction in the viscosity of the CNC-LS dispersion, confirming that mostly all CNC particles are being transported through the porous media, and

the main part of the pressure build-up is linked to the filtration of the largest fraction of CNC particles at the inlet surface. The effluent viscosity measurements are shown in Figure 3.1.

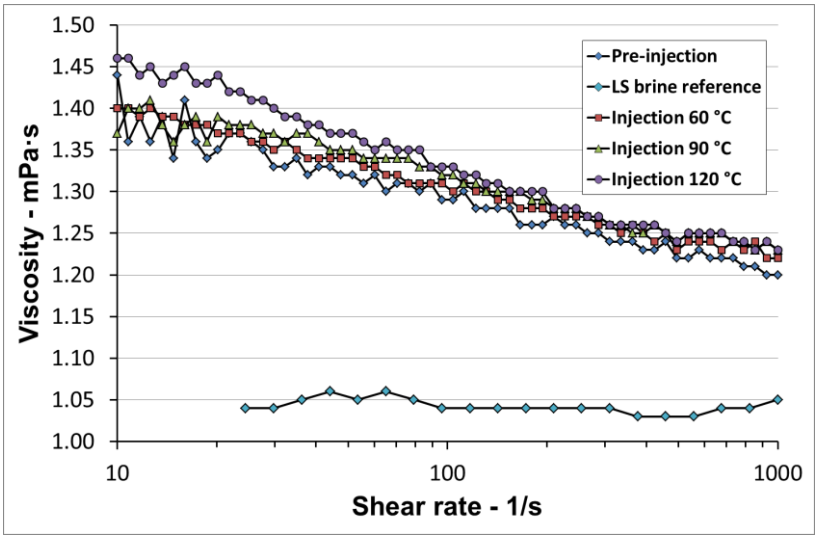

Figure 3.1: Core flooding with 0.5 wt. % CNC-LS brine into core SM8 at 60, 90 and 120 °C. The viscosity of effluent samples was measured and compared with the viscosity of a pre-flooded CNC-LS sample. Measurements were performed at increasing shear rates at 20 °C.

The core SM8 was regenerated for the next test by flooding the core with LS brine in the reversed direction, to remove CNC particles from inside the core and from the inlet surface. LS brine flooding confirmed only slight changes in core permeability on the regenerated core. The CNC-LS flooding test was repeated at both 90 and 120 °C. The pressure build-up effects are presented in Figure 3.2.

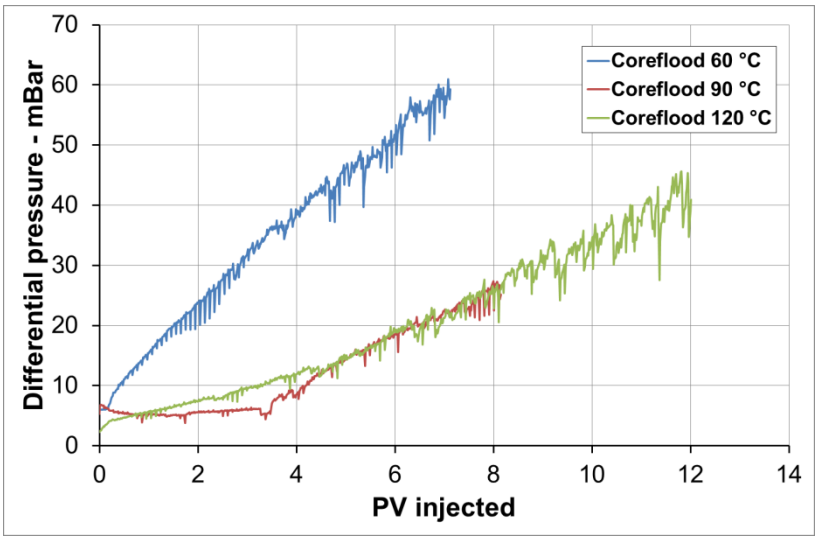

Figure 3.2: Core flooding of a 100 % LS saturated sandstone core SM8. The core was flooded with 0.5 wt. % CNC-LS brine at a rate of 4 PV/Day at 60, 90, and 120 °C. Pressure drop (ΔP) over the core was measured as a function of PV injected.

Less pressure build-up is observed at 90 and 120 °C compared to 60 °C. The viscosity of effluent samples at 90 and 120 °C are also in line with the effluent viscosity at 60 °C, confirming that the major part of the viscosity-contributing CNC particles is transported through the porous media at all tested temperatures, indicated in Figure 3.1. At a shear rate of 10 1/s, the effluent viscosity at 60, 90 and 120 °C is close to 1.40 mPa·s, while the viscosity of the bulk dispersion is 1.45 mPa·s. In a previous study, the viscosity of the CNC-LS solution significantly increased during long term temperature aging (Molnes et al., 2017). No increase in the viscosity of CNC-LS effluent viscosity were observed during these experiments. A possible explanation for this is that the CNC particles are not trapped in the pore matrix long enough for the viscosity increase to take place. At an injection rate of 4 PV/day, a CNC particle will use approximately 6 hours to travel through the core. The heat aging experiments revealed that this increase in viscosity is not observed before the dispersion has been aged for at least 20 hours (Molnes et al., 2017). On a lab scale, the time frame is thus too short to observe these viscosity changes, but on oil reservoir scale, there is a possibility that this heat viscosifying effect may increase the viscosity of the CNC-LS solution giving an extra support to the oil recovery process.

The core permeability in the different experiments is given in Table 3.1. Permeability values in mD were acquired using Equation 2.1.

Table 3.1: Permeability of core SM8 after core cleaning/core regeneration, and prior to injectivity tests (K_1) at 60, 90 and 120 °C. K_2 indicates the calculated values between measurements, after regeneration.

Temperature, °C	K_1, mD	K_2, mD
60	63	44
90	44	75
120	75	68

As observed after the 90 °C CNC-LS injection, the permeability of the core sample was increased. This was not expected, as earlier injection studies with CNC-LS generally exhibited a decrease in permeability, due to particles trapped inside the porous medium (Molnes et al., 2016). The reason for this effect may be a beginning degradation of CNC trapped in the porous media. Prolonged exposure to high temperatures can change the surface chemistry of the CNC, for example by release of sulphate ester groups (Molnes et al., 2017), and this change may lead to desorption/un-jamming of trapped CNC. Combined with an elevated injection rate between the measurements, the CNC particles are probably expelled from the core sample.

The increase in differential pressure over the core SM8 is mainly caused by filtering at the core inlet, but some adsorption on pore surfaces or jamming in pore throats cannot be excluded. As mentioned in the Introduction, the CNC particles are negatively charged, due to the sulphate half esters substitutions on their surfaces through the production process. Silicate

minerals in the pore surfaces are also negatively charged, which excludes electrostatic adsorption.

The pH values in the effluent samples were also tested. It is known that brine pH of non-buffered systems can increase when flooded through sandstone, due to a cation exchange reaction with pore surface minerals, where H^+ exchange with cations at mineral surfaces (Austad et al., 2010). The bulk pH of the CNC-LS brine was 5.7, as shown in Figure 3.3.

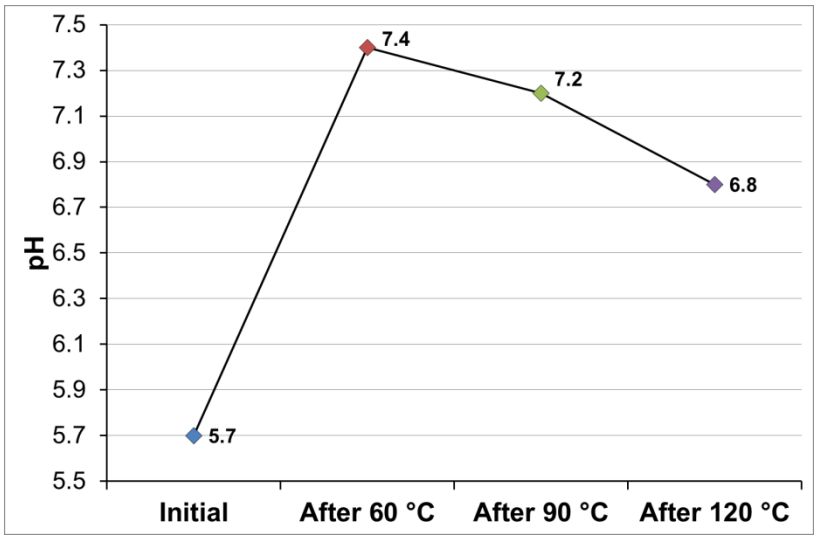

Figure 3.3: pH of 0.5 wt% CNC-LS brine samples, before injection and in effluent samples after core flooding at 60, 90 and 120 °C.

As seen in the figure, the pH observed in CNC-LS effluent samples at 60, 90 and 120 °C confirmed a ΔpH of 1.7, 1.5 and 1.1 respectively. The results are in agreement with reduced pH changes during LS brine injection in sandstone cores at increasing temperatures (Piñerez Torrijos et al., 2016).

The observed effluent pH could also be affected by the chemistry of CNC, like sulphate ester groups being split off (Dorris & Gray, 2012; Heggset et al., 2017; Molnes et al., 2017).

3.2 Oil recovery experiments

Enhanced oil recovery experiments were performed both at 60 and 90 °C using sandstone core SM10. After a mild core cleaning, the core was restored with S_{wi} = 20 %, and saturated and aged in crude oil. The tests were performed by initially LS injection (secondary mode) until ultimate oil recovery plateau was reached, before the CNC-LS solution was injected in tertiary mode.

The results from the oil recovery test performed at 90 °C are shown in Figure 3.4.

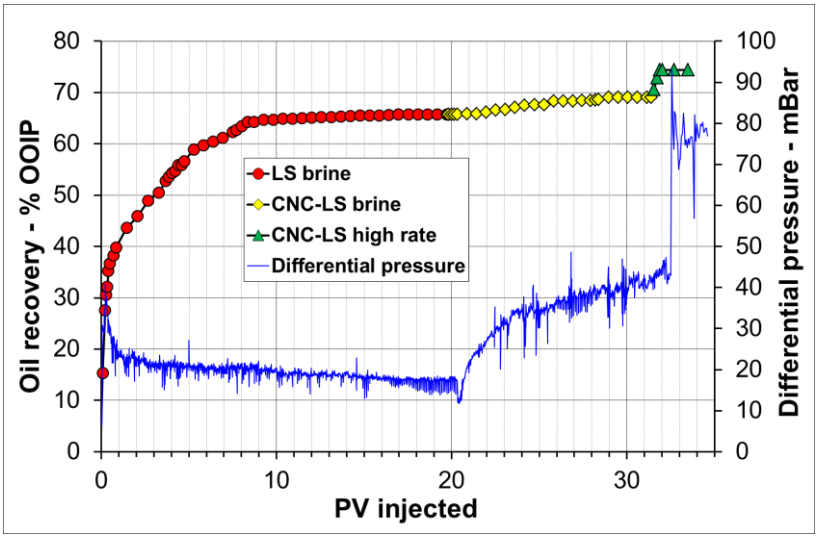

Figure 3.4: Oil recovery test performed on core SM10 at 90 °C. The core with S_{wi} = 0.2 and saturated and aged with crude oil, was successively flooded with LS – CNC-LS brines a rate of 4 PV/Day. The oil recovery (% OOIP) and ΔP (mBar) are shown as a function of PV injected (time). At the end, the injection rate was increased to 16 PV/Day.

During secondary LS brine injection, the oil recovery steadily increased, and an ultimate recovery plateau of 66 % OOIP was reached after 8 PV injected. The LS recovery result is in line with the observed results by (Piñerez Torrijos et al., 2016).

The ΔP gradually decreased as the water saturation of the core increased. A fluctuation in ΔP was observed during LS injection, which is an indication that mobile oil is moving through the pore throats. The ΔP fluctuation decreased when the ultimate recovery was reached. 19 PV of LS brine was injected to ensure that all mobile oil was produced.

When the CNC-LS brine was injected, an increase in differential pressure was observed. During the next 11 PV, 3.4 % OOIP extra oil was produced. In the same period, there was also observed an increase in the ΔP fluctuation, which could indicate increased mobilisation of oil in the pore space due to the introduction of CNC particles. At the end, the injection rate was increased 4 times to 16 PV/day. Differential pressure increased significantly with increased injection rate and an extra oil production of 5.4 % OOIP was obtained. The pH of the bulk CNC-LS dispersion was 5.7, and the pH measured in sampled CNC-LS effluent was 7.4.

Oil recovery studies on the same CoBR system, confirms reproducible ultimate recoveries during secondary FW injections in the range of 35 – 40 % OOIP at 60 – 120 °C, which are explained by low pH of produced water (PW) which is not promoting wettability alteration and increased microscopic sweep efficiency (Piñerez Torrijos et al., 2016). Compared to the ultimate oil recovery plateau of 66% and pH increase observed during secondary LS injections, the effect of improved microscopic sweep efficiency could have a dramatic effect

on the amount of producible oil from heterogeneous pore structures, and the tertiary CNC—LS injection at 90 °C was able to improve the ultimate recovery from 66 – 69.4 % OOIP.

A second oil recovery experiment was performed on core SM10 at 60 °C, also using CNC-LS in tertiary mode after LS injection. The results from the test is presented in figure 3.5.

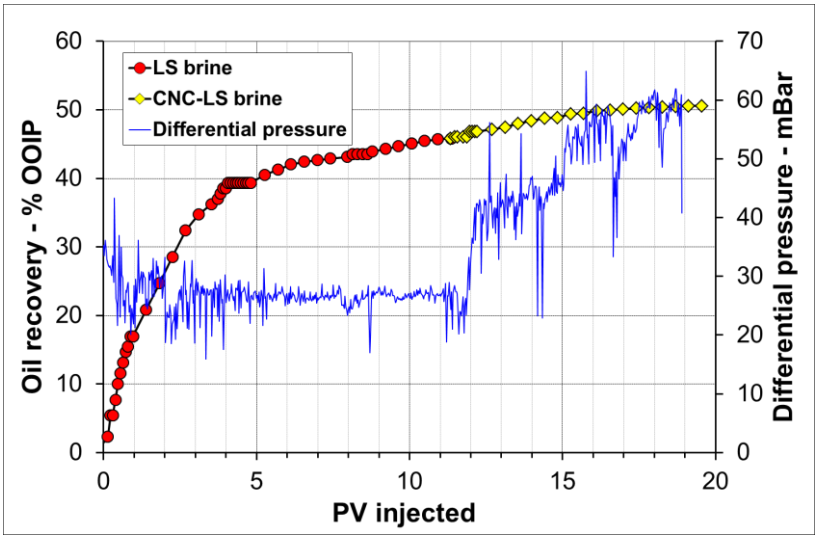

Figure 3.5: Oil recovery test performed on core SM10 at 60 °C. The core with S_{wi}=0.2 and saturated and aged in crude oil, was successively flooded with LS – CNC-LS brines a rate of 4 PV/Day. The Oil recovery (%OOIP) and the ΔP (mBar) are reported as a function of PV injected (time).

During the LS injection, the oil recovery gradually increased and reached 45.8 %OOIP after 11 PV. Fluctuation in ΔP indicated oil production. After 5 PV injected, the differential pressure fluctuations stabilised as the oil production decreased. Compared to the experiment performed at 90 °C and previous LS EOR experiments performed on the same CoBR system, the LS brine only improved the oil recovery from 40 % OOIP, which are expected as base line recovery without wettability alteration using FW, to 45.8 % OOIP after 11 PV injected. In this experiment, the LS brine failed to contribute with an efficient wettability alteration and increased microscopic sweep efficiency.

At 11 PV, the injection brine was changed to CNC-LS. At the changing point the core was less water wet compared to the experiments observed after LS injection at 90 °C and at 60 °C by (Piñerez Torrijos et al., 2016). As the CNC-LS brine was injected, the differential pressure increased with increased fluctuations, Figure 3.4. The introduction of CNC particles into the pores space affects the fluid flow in the pores, and log jamming of CNC particles in pore throats and redistribution of oil could be an explanation of the observations. At less water wet conditions, the CNC-LS injection is not contributing with a significant increased recovery

compared to LS injection. The experiment was terminated after 20 PV injected, with an ultimate oil recovery of 51 % OOIP. Table 3.2 shows the measured pH values for the bulk LS brine and CNC-LS dispersion prior to injection, and pH values of the produced water samples during LS and CNC-LS injection.

Table 3.2: pH measured in bulk solutions and produced water samples at 60 °C.

Sample	Bulk pH	Effluent pH	ΔpH
LS brine	5.8	7.6	1.8
CNC-LS	5.6	6.4	0.8

A less pH increase is observed in PW samples during CNC-LS injection compared to LS brine, and this may indicate that the CNC-LS brine is less efficient as a wettability modifier. It may also be that the pH is influenced by desulfation (Dorris & Gray, 2012).

For both experiments, a fluctuation in differential pressure over the core was observed during CNC-LS injection in tertiary mode, which may be a sign of log jamming and redistribution of oil within the pore space. The pores are in the range from 0.01 to 100 µm, with the majority at 10 µm. According to Zhong et al. (2012), CNC can form agglomerates of approx. 1 µm at a Na^+ salinity of 50 mM. Agglomeration may also be promoted by reduced surface charge due to desulfation at the elevated temperature with reduced repulsion of particles as a result. Log jamming is thus likely. An increase in pH was seen for the CNC-LS dispersion at both test temperatures, with the largest increase observed at 90 °C, with a Δ pH of 1.7. At 60 °C, the Δ pH was 0.8. The large jump at 90 °C is most likely caused by changes in the reactivity of the CNC particles with increasing temperature. The rock minerals contribute with the same pH increase during LS injection at both 60, 90, 120 °C (Piñerez Torrijos et al., 2016).
As discussed, the CNC particles could cause water diversion by jamming up in easily flooded pore throats, which could lead the water flow diversion into less available pores.

4. Conclusions

The injectivity of CNC-LS brine into sandstone cores have been studied at 60, 90 and 120 °C. The CNC particles were injectable at all studied temperatures. Rheological measurements of effluent samples confirmed that the main part of CNC particles travelled through the core material. The increase in differential pressure was substantially lower at 90 and 120 °C, compared to 60 °C. Core regeneration by injecting low saline brine in reverse confirmed that most of the retained particles were filtered on the inlet of the core, and that only small changes in core permeability was observed. The particle size of the CNC should be optimised to reduce the observed filtration on the core inlet. Oil recovery tests with CNC-LS brine used in tertiary

mode after LS injection showed that the CNC dispersion affect fluid flow in the pores. As the CNC dispersion was injected, increased fluctuation in the differential pressure over the core was observed.

The oil recovery experiment performed at 90 °C showed a small but significant tertiary CNC-LS EOR effect of 3.4 %OOIP, after a secondary LS injection promoting an efficient wettability alteration towards more water wet conditions. Without an efficient wettability alteration during the LS injection, no significant EOR effect during tertiary CNC-LS was observed in the oil recovery test performed at 60 °C. The preliminary results indicate that CNC particles may have some potential as a green flooding fluid additive, but that more investigation is needed.

At this early stage of research, it is difficult to suggest a mechanism behind the extra oil observed. The CNC particles could participate in log jamming and agglomeration in pore throats, as the core floodings showed increased pressure drop fluctuations during CNC-LS injection. Both the CNC particles and the silicate minerals present in the cores are negatively charged at typical reservoir pH, and further studies should include CNC particles with modified surface charges which could affect log jamming and diverted flow. The chemistry of the CNC particles also effected the CoBR chemistry which are important in explaining wettability and wettability alteration processes as observed during FW and LS brine injection.

Acknowledgements

This work was performed as a part of the NORCEL Project: The NORwegian NanoCELlulose Technology Platform, initiated and led by The Paper and Fibre Research Institute (PFI) in Trondheim and funded by the Research Council of Norway through the NANO2021 Program, grant number 228147. The experimental work in this study has been carried out at the University of Stavanger (UoS) in the Smart Water EOR laboratory facilities, which is a part of the Department of Petroleum Technology, and at the Ugelstad Laboratory, which is part of the Department of Chemical Engineering at the Norwegian University of Science and Technology (NTNU).

References

(ASTM), A. S. f. T. M. (1988). Standard test method for base number of petroleum products by potentiometric perchloric acid titration. *Annual Book of ASTM Standards* (Vol. ASTM D2896-88). West Conshohocken, PA, USA: ASTM International.

(ASTM), A. S. f. T. M. (1989). Standard test method for acid number of petroleum products by potentiometric titration. *Annual Book of ASTM Standards* (Vol. ASTM D664-89). West Conshohocken, PA, USA: ASTM International.

Aadland, R. C., et al. (2016). INJECTIVITY AND RETENTION OF NANOCELLULOSE DISPERSIONS IN BEREA SANDSTONE.

Aguiar, J., & Mansur, C. (2016). THE INFLUENCE OF POLYMER FLOODING ON PRODUCED OILY WATER: A REVIEW. *Brazilian Journal of Petroleum and Gas, 10*(1).

Austad, T., et al. (2010). *Chemical mechanism of low salinity water flooding in sandstone reservoirs.* Paper presented at the SPE improved oil recovery symposium.

Bao, M., et al. (2010). Biodegradation of partially hydrolyzed polyacrylamide by bacteria isolated from production water after polymer flooding in an oil field. *Journal of hazardous materials, 184*(1), 105-110.

Beal, C. (1946). The Viscosity of Air, Water, Natural Gas, Crude Oil and Its Associated Gases at Oil Field Temperatures and Pressures. *Transactions of the AIME 165*(1), 94-115. doi:10.2118/946094-G

Bolandtaba, S. F., et al. (2009). *Pore scale modelling of linked polymer solution (LPS)–A new EOR process.* Paper presented at the IOR 2009-15th European Symposium on Improved Oil Recovery.

Dorris, A., & Gray, D. G. (2012). Gelation of cellulose nanocrystal suspensions in glycerol. *Cellulose, 19*(3), 687-694.

Fan, T., & Buckley, J. S. (2006). *Acid number measurements revisited.* Paper presented at the SPE/DOE Symposium on Improved Oil Recovery.

Guo, Y. (2013, 06.11.13). *Environmental Aspect of EOR Chemicals.* Paper presented at the FORCE - EOR Competence Buiding Workshop, Stavanger.

Habibi, Y., et al. (2010). Cellulose nanocrystals: chemistry, self-assembly, and applications. *Chemical Reviews, 110*(6), 3479-3500.

Heggset, E. B., et al. (2017). Temperature stability of nanocellulose dispersions. *Carbohydrate Polymers, 157*, 114-121. doi:http://dx.doi.org/10.1016/j.carbpol.2016.09.077

Hendraningrat, L., et al. (2013). A coreflood investigation of nanofluid enhanced oil recovery. *Journal of Petroleum Science and Engineering, 111*, 128-138.

Hu, Z., et al. (2016). Nanoparticle-Assisted Water-Flooding in Berea Sandstones. *Energy & Fuels*. doi:10.1021/acs.energyfuels.6b00051

Jahn, F., et al. (2008). Reservoir Description *Hydrocarbon Exploration and Production* (2nd ed., pp. 95-171). Amsterdam: Elsevier.

Kamal, M. S., et al. (2015). Review on polymer flooding: rheology, adsorption, stability, and field applications of various polymer systems. *Polymer Reviews, 55*(3), 491-530.

Kjøniksen, A.-L., et al. (2008). Modified polysaccharides for use in enhanced oil recovery applications. *European Polymer Journal, 44*(4), 959-967.

Klemm, D., et al. (2011). Nanocelluloses: A New Family of Nature-Based Materials. *Angewandte Chemie International Edition, 50*(24), 5438-5466. doi:10.1002/anie.201001273

Lafitte, V., et al. (2014). Fluids and Methods Including Nanocellulose: Google Patents.

Lager, A., et al. (2007). *Impact of brine chemistry on oil recovery.* Paper presented at the IOR 2007-14th European Symposium on Improved Oil Recovery.

Ligthelm, D. J., et al. (2009). *Novel Waterflooding Strategy By Manipulation Of Injection Brine Composition.* Paper presented at the EUROPEC/EAGE Conference and Exhibition.

574 Liu, F., et al. (2012). *Optimizing Water Injection Rates for a Water-flooding Field.* Paper presented at
575 the SPE Annual Technical Conference and Exhibition.
576 McGuire, P., et al. (2005). *Low salinity oil recovery: An exciting new EOR opportunity for Alaska's North*
577 *Slope.* Paper presented at the SPE Western Regional Meeting.
578 Molnes, S. N., et al. (2017). The effects of pH, time and temperature on the stability and viscosity of
579 cellulose nanocrystal (CNC) dispersions: implications for use in enhanced oil recovery.
580 *Cellulose*, 1-13. doi:10.1007/s10570-017-1437-0
581 Molnes, S. N., et al. (2016). Sandstone injectivity and salt stability of cellulose nanocrystals (CNC)
582 dispersions—Premises for use of CNC in enhanced oil recovery. *Industrial Crops and Products,*
583 *93*, 152-160. doi:http://dx.doi.org/10.1016/j.indcrop.2016.03.019
584 Muggeridge, A., et al. (2014). Recovery rates, enhanced oil recovery and technological limits.
585 *Philosophical Transactions of the Royal Society A: Mathematical,*
586 *Physical and Engineering Sciences, 372*(2006). doi:10.1098/rsta.2012.0320
587 OSPAR. (2016). OSPAR List of Substances Used and Discharged Offshore which Are Considered to Pose
588 Little or No Risk to the Environment (PLONOR) – Update 2016. Retrieved from
589 http://www.ospar.org/work-areas/oic/chemicals
590 Piñerez Torrijos, I. D., et al. (2016). Experimental Study of the Response Time of the Low-Salinity
591 Enhanced Oil Recovery Effect during Secondary and Tertiary Low-Salinity Waterflooding.
592 *Energy & Fuels, 30*(6), 4733-4739. doi:10.1021/acs.energyfuels.6b00641
593 Raney, K. H., et al. (2012). Surface and subsurface requirements for successful implementation of
594 offshore chemical enhanced oil recovery. *SPE Production & Operations, 27*(03), 294-305.
595 Reiner, R. S., & Rudie, A. W. (2013). Process Scale-Up of Cellulose Nanocrystal Production to 25 kg per
596 Batch at the Forest Products Laboratory. In M. T. Postek, R. J. Moon, A. W. Rudie, & M. A.
597 Bilodeau (Eds.), *Production and Applications of Cellulose Nanomaterials* (pp. 21-24). Peachtree
598 Corners, GA, USA: TAPPI Press.
599 Revol, J.-F., et al. (1992). Helicoidal self-ordering of cellulose microfibrils in aqueous suspension.
600 *International Journal of Biological Macromolecules, 14*(3), 170-172.
601 Rincon-Torres, M. T., & Hall, L. J. (2015). Cellulose nanowhiskers in well services: Google Patents.
602 Sacui, I. A., et al. (2014). Comparison of the properties of cellulose nanocrystals and cellulose
603 nanofibrils isolated from bacteria, tunicate, and wood processed using acid, enzymatic,
604 mechanical, and oxidative methods. *ACS applied materials & interfaces, 6*(9), 6127-6138.
605 Seccombe, J., et al. (2010). *Demonstration of low-salinity EOR at interwell scale, Endicott field, Alaska.*
606 Paper presented at the SPE Improved Oil Recovery Symposium.
607 Seright, R. S., & Henrici, B. J. (1990). Xanthan Stability at Elevated Temperatures. *SPE reservoir*
608 *engineering, 5*(1), 52-60. doi:10.2118/14946-PA
609 Sheng, J. J., et al. (2015). Status of polymer-flooding technology. *Journal of Canadian Petroleum*
610 *Technology, 54*(02), 116-126.
611 Skauge, A. (2008). *Microscopic diversion-A new EOR technique.* Paper presented at the The 29th IEA
612 Workshop & Symposium, Beijing, China.
613 Skauge, T., et al. (2010). *Nano-sized particles for EOR.* Paper presented at the SPE Improved Oil
614 Recovery Symposium.
615 Springer, N., et al. (2003). *Resistivity index measurement without the porous plate: A desaturation*
616 *technique based on evaporation produces uniform water saturation profiles and more reliable*
617 *results for tight North Sea chalk.* Paper presented at the Proceedings of the International
618 Symposium of the Society of Core Analysts.
619 Strand, S., et al. (2016). Water based EOR from clastic oil reservoirs by wettability alteration: A review
620 of chemical aspects. *Journal of Petroleum Science and Engineering, 146*, 1079-1091.
621 Taber, J. J., et al. (1997). EOR screening criteria revisited-Part 1: Introduction to screening criteria and
622 enhanced recovery field projects. *SPE reservoir engineering, 12*(03), 189-198.

623 Tang, G.-Q., & Morrow, N. R. (1999a). Influence of brine composition and fines migration on crude
624 oil/brine/rock interactions and oil recovery. *Journal of Petroleum Science and Engineering,*
625 *24*(2), 99-111.
626 Tang, G.-q., & Morrow, N. R. (1999b). Oil recovery by waterflooding and imbibition—invading brine
627 cation valency and salinity. *Paper SCA9911*.
628 Thomas, S. (2008). Enhanced Oil Recovery - An Overview. *Oil & Gas Science and Technology - Revue*
629 *de l'IFP, 63*(1), 9-19.
630 Torrijos, I. D. P., et al. (2017). Impact of temperature on the low salinity EOR effect for sandstone cores
631 containing reactive plagioclase. *Journal of Petroleum Science and Engineering, 156*, 102-109.
632 Wei, B., et al. (2016). The Potential of a Novel Nanofluid in Enhancing Oil Recovery. *Energy & Fuels,*
633 *30*(4), 2882-2891.
634 Wellington, S. L. (1983). Biopolymer solution viscosity stabilization-polymer degradation and
635 antioxidant use. *Society of petroleum engineers journal, 23*(06), 901-912.
636 Wever, D., et al. (2011). Polymers for enhanced oil recovery: a paradigm for structure–property
637 relationship in aqueous solution. *Progress in Polymer Science, 36*(11), 1558-1628.
638 Zhong, L., et al. (2012). Colloidal stability of negatively charged cellulose nanocrystalline in aqueous
639 systems. *Carbohydrate Polymers, 90*(1), 644-649.
640 Zolotukhin, A. B., & Ursin, J.-R. (2000). Permeability *Introduction to Petroleum Reservoir Engineering*
641 (pp. 63-82). Kristiansand: Norwegian Academic Press (HøyskoleForlaget).

642

643